Effects of hydrostatic pressure and temperature on the electron paramagnetic resonance spectrum of off-centre Jahn–Teller $[CuF_4F_4]^{6-}$ complexes in SrF_2 crystal

2003 J. Phys.: Condens. Matter 15 1081

(http://iopscience.iop.org/0953-8984/15/7/306)

INSTITUTE OF PHYSICS PUBLISHING JOURNAL OF PHYSICS: CONDENSED MATTER

J. Phys.: Condens. Matter **15** (2003) 1081–1096 PII: S0953-8984(03)52185-3

Effects of hydrostatic pressure and temperature on the electron paramagnetic resonance spectrum of off-centre Jahn–Teller $[CuF_4F_4]^{6-}$ complexes in SrF_2 crystal

V A Ulanov[1,3], M Krupski[2], S K Hoffmann[2] and M M Zaripov[1]

[1] Physical Technical Institute, Russian Academy of Sciences, Sibirski Trakt 10/7, 420029 Kazan, Russia
[2] Institute of Molecular Physics, Polish Academy of Sciences, Smoluchowskiego 17, PL-60-179 Poznan, Poland

E-mail: ulanov@dionis.kfti.kcn.ru

Received 9 August 2002, in final form 10 January 2003
Published 10 February 2003
Online at stacks.iop.org/JPhysCM/15/1081

Abstract

Pressure and temperature variations of the spin-Hamiltonian parameters and electron paramagnetic resonance (EPR) linewidths of non-central Jahn–Teller $[CuF_4F_4]^{6-}$ complexes in SrF_2 crystal were studied by continuous-wave EPR. It was found that the static spin-Hamiltonian parameters, found at $T = 85$ K and at normal pressure ($g_\parallel = 2.491$, $g_\perp = 2.083$, $a_\parallel = 360$, $a_\perp = 26$, $A_{x''} = 96$, $A_{y''} = 99$, $A_{z''} = 403$ and $\beta_{exp} = 17°$), are slightly changed with hydrostatic pressure and, at $T = 85$ K and $P = 550$ MPa, become equal to $g_\parallel = 2.489$, $g_\perp = 2.083$, $a_\parallel = 348$, $a_\perp = 27$, $A_{x''} = 99$, $A_{y''} = 102$, $A_{z''} = 406$ and $\beta_{exp} = 20°$ (a and A values in megahertz, x''-, y''- and z''-axes are eigenvectors of the super-hyperfine tensor A, β_{exp} is the experimental value of the angle between the C_4 symmetry axis of the complex and the x''-axis). With increasing temperature the well-resolved EPR spectrum of the complex is transformed continuously into a single broad line both at normal pressure and at a hydrostatic pressure of 550 MPa. But in the first case the coalescence point corresponds to 220–230 K while in the second case it is 195–205 K. Treatment using the linear combination of atomic orbitals representation of molecular orbitals (LCAO MO) model was performed to establish some relations between variations of the spin-Hamiltonian parameters and pressure-induced changes in the molecular structure of the complex. To get some additional information about the molecular structure of the complex and variations of its structural parameters with pressure, treatment using the rigid-ion model was performed. Experimental and theoretical results are discussed in the framework of the Jahn–Teller model of the complex.

[3] Author to whom any correspondence should be addressed.

1. Introduction

In this paper we report experimental results on the influence of hydrostatic pressure on the static spin-Hamiltonian parameters and interwell transition rates of non-central impurity Jahn–Teller $[CuF_4F_4]^{6-}$ complexes in an SrF_2 crystal lattice. Our previous investigations of these complexes performed by continuous-wave (cw) [1] and pulsed [2] electron paramagnetic resonance (EPR) methods gave us rather detailed information about some of their physical properties. By analysing the angular dependences in the hyperfine (HF) and super-hyperfine (SHF) structures of the cw EPR spectra the equilibrium positions of copper and fluorine nuclei were estimated in [1]. Temperature dependences of the spin–lattice relaxation rate, $1/T_1$, and the phase memory time, T_M, were determined (in the temperature range 4.2–100 K under normal pressure) in our previous work [2]. As was found in [1], the static nuclear configuration of $[CuF_4F_4]^{6-}$ in SrF_2 corresponds to a tetragonally distorted cube with the fluorine ions at the vertices of this cube and the impurity copper ion in its body (figure 1). The position of the impurity copper is strongly non-central; it is shifted along the C_{4v} symmetry axis from the centre of its coordinational polyhedron by a distance of about 0.1 nm. Thus, the impurity complex has a six-well adiabatic potential and its physical properties are expected to be strongly temperature dependent. Some of the dependences were observed explicitly in our pulsed EPR study [2]. It was found that the electron spin–lattice relaxation rate $1/T_1$ grows rapidly on heating, by six orders of magnitude in the temperature range 4.2–100 K, and its temperature dependence can be described by an Orbach-type process with excitations to two excited states of energy, 83 and 174 cm^{-1}. At temperatures higher than 150 K this relaxation rate is dominated by over-barrier jumps (this fact is observed explicitly using the cw EPR method which demonstrates the appearance of an isotropic EPR spectrum above $T = 225$ K). All experimental results mentioned above have led us to the following conclusion. A Jahn–Teller effect of the $(T_{2g} \times A_{2u}) \otimes (a_{1g} + e_g + t_{1u})$ type produces six equivalent wells on the surface of the lowest adiabatic potential sheet. Every adiabatic well corresponds to one of the six possible off-centre shifts of the Cu^{2+} ion. Any off-centre shift of a copper impurity is accompanied by a suitable $O_h \rightarrow C_{4v}$ distortion of the coordination cube. At temperatures below 30 K the $[CuF_4F_4]^{6-}$ complex is mainly localized within one of the six adiabatic wells on the ground vibronic level. Of course, there is some possibility of the complex crossing a potential barrier and coming into an adjacent well, but, as follows from our previous experiments [2], such a possibility of a tunnelling process from the ground vibronic level is very low. This process is facilitated when the complex occurs on an excited vibronic level. The energies of the two lowest excited vibronic levels were estimated in [2] as $E_1 \approx 83$ cm^{-1} and $E_2 \approx 174$ cm^{-1}.

It must be noted that there are two types of potential barrier between the six equivalent adiabatic wells of the $[CuF_4F_4]^{6-}$ complex. The first corresponds to a transition of the copper ion via the centre of its coordination cube and, consequently, to a transition between two adiabatic wells having antiparallel vectors of the off-centre shift. The second type of barrier is between adjacent adiabatic wells with orthogonal shift vectors. As follows from the Born–Mayer model calculations (a short description of which will be presented in section 4), the first type of barrier is much higher than the second type.

It was very interesting to compare the properties of impurity copper complexes embedded into some lattices of fluorite-type crystals. Such a review (see, for instance, [2] and references therein) allowed us to suppose that the static and dynamic properties of the $[CuF_4F_4]^{6-}$ complex in SrF_2 crystals must be very sensitive to external pressure. In fact, it was found using the cw EPR method [3] that symmetry of the lattice distortions arising around a ^{2S+1}D impurity ion in an eightfold coordinated position in fluorite-type lattices depends on the parameter

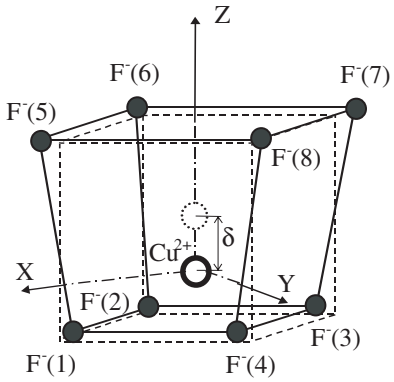

Figure 1. Molecular structure of the Jahn–Teller $[CuF_4F_4]^{6-}$ impurity complex in an SrF_2 crystal (coordination cube of the Sr^{2+} replaced by an impurity copper ion is shown by dashed lines; δ determines a shift of the Cu^{2+} ion into an equilibrium position; fluorine positions are represented qualitatively taking into account results of the rigid-ion model calculations described briefly in section 4.1).

$$\eta = \frac{4(r_{imp} + r_{an})}{\sqrt{3}a_0} \tag{1}$$

where a_0 is the size of the coordinational cube of the alkaline-earth cation which was replaced by the impurity ion and r_{imp} and r_{an} are the ionic radii of the $^{2S+1}$D impurity and fluorine ions respectively. Three types of nuclear configuration are realized for the impurity paramagnetic complex depending on the η-value:

(i) A trigonally distorted coordination cube with an impurity ion in the central position ($[MeF_2F_6]^{6-}$, D_{3d}). This is realized for $\eta \geqslant 0.83$.
(ii) An orthorhombically distorted coordination cube with an impurity ion in its centre ($[MeF_4F_4]^{6-}$, D_{2h}), for $0.79 < \eta < 0.83$.
(iii) A non-central impurity complex ($[MeF_4F_4]^{6-}$, C_{4v}), for $\eta \leqslant 0.79$.

In the last case each impurity ion is strongly shifted (∼0.1 nm) along a C_4 axis of its coordination cube. Such a significant shift was also observed for Cu^{2+} ($3d^9$, ^{2}D) and Ag^{2+} ($4d^9$, ^{2}D) ions in $SrCl_2$ (fluorite-type) crystals [4–6], and for Ni^+ ($3d^9$, ^{2}D) ions in CaF_2 [7] and SrF_2 [8]. We have no information available on the ionic radius of Cu^{2+} in the eightfold coordination position, but we can evaluate it approximately from data on fourfold ($r_4(Cu^{2+}) = 0.62$) and sixfold ($r_6(Cu^{2+}) = 0.73$) coordination positions [9]. Taking $r_8(Cu^{2+}) = 0.65$–0.69, $r_F = 1.31$ and $a_0 = 5.80$, we can get $\eta = 0.780$–0.796. Thus, as this is very close to the critical value $\eta \approx 0.79$, we can hope in the present study to detect an influence of hydrostatic pressure on the static and dynamic features of the cw EPR spectra of the $[CuF_4F_4]^{6-}$ complex in an SrF_2 crystal.

Section 2 of the present paper contains a short description of the experimental techniques used in the study. The experimental results are presented in section 3. Section 4, divided into two parts, is devoted to a theoretical treatment of the experimental results obtained in this study and a discussion. Pressure dependences of static Zeeman and SHF interaction parameters are treated theoretically and discussed in section 4.1. As these spin-Hamiltonian parameters depend on structural parameters of the impurity complex (the Euler angle coordinates of the nuclei and 'impurity–ligand' distances), some effort was made to derive the relations between these two groups of parameters. A short account of this treatment made using the angular

overlap model (AOM) approach (AOM linear combination of atomic orbitals representation of molecular orbitals (AOM LCAO MO); see, for example, [10]) and the rigid-ion model of ionic crystals [11] is given in section 4.1. The experimental data for the influence of hydrostatic pressure on the cw EPR line widths are discussed in section 4.2. Section 5 is devoted to general conclusions.

2. Experimental details

Continuous-wave EPR experiments under hydrostatic pressure were performed at the Institute of Molecular Physics (Poznan) in a specially designed high-pressure appliance [12]. This was a cylindrical corundum resonator tuned in the TE_{112} mode. The resonator is coupled to a microwave (x-band) coaxial line and placed inside a reinforced pressure chamber made of beryllium bronze. Using this equipment it is possible to perform a high-pressure experiment up to 800 MPa in the temperature range 80–400 K. The pressure of the transferring liquid is produced within the steel high-pressure cylinder and delivered to the pressure chamber via a capillary. Petroleum ether is used as the pressure-transmitting medium. The pressure is monitored with a standard manometer to the accuracy of 2 MPa. The desired temperature is established within the chamber by adjusting the rate of liquid nitrogen flow through the heat exchanger placed immediately upon the pressure chamber. The temperature is controlled with an accuracy of better than 0.1 K and measured with a copper–constantan thermocouple. The 80 Hz magnetic field modulation is provided by the modulation coils mounted outside the pressure chamber.

The SrF_2:Cu^{2+} crystals were grown by the Bridgman method in a conical graphite crucible in a helium atmosphere with the addition of a small amount of fluorine gas. The copper impurity was introduced in the melt as a well-dried copper fluoride (CuF_2) powder. The samples were treated to get a crystalline rod (of 1.5 mm diameter and 8 mm length) with the axis parallel to the [110] crystal axis. This rod was placed at the centre of corundum resonator with the cylindrical axis of the rod perpendicular to the direction of the external static magnetic field. The cylindrical sample was rotated about its [110] axis and rotation angles were obtained from an analysis of the EPR spectra recorded at normal pressure. Due to the well-resolved hyperfine structure (HFS) and super-hyperfine structure (SHFS) of the EPR spectra these angles were determined with an accuracy of better than 1°.

3. Experimental results

The spin-Hamiltonian describing the angular dependences of the resonance EPR line positions of a $[CuF_4F_4]^{6-}$ impurity complex in SrF_2 crystals can be represented in the form

$$H_S = \beta_e B_0 g S + S a I^{\mathrm{Cu}} + I^{\mathrm{Cu}} Q I^{\mathrm{Cu}} - g_N^{\mathrm{Cu}} \beta_N B_0 I^{\mathrm{Cu}} + \sum_{i=1}^{4} (S A_i I_i^{\mathrm{F}} - g_N^{\mathrm{F}} \beta_N B_0 I_i^{\mathrm{F}}), \tag{2}$$

where β_e and β_N are the electron and nuclear magnetons, g, a and A_i are 3×3 matrices describing anisotropy of the electron Zeeman, HF and SHF interactions (so-called g, HF and SHF tensors) respectively, Q is the quadrupole tensor, g_N^{Cu} and g_N^{F} are the nuclear g-factors ($g_N^{^{63}\mathrm{Cu}} = 1.484$ and $g_N^{\mathrm{F}} = 5.2577$), I^{Cu} and I_i^{F} the nuclear spin operators (i runs over the numbers of fluorine nuclei displaying a well-resolved SHF structure in the EPR spectra) and S is the electron spin operator.

It is convenient to present the spin-Hamiltonian (2) in the coordinate system (X, Y, Z) with $X \parallel \langle 110 \rangle$, $Y \parallel \langle -110 \rangle$, and $Z \parallel C_{4v} \parallel \langle 001 \rangle$ (where C_{4v} is the symmetry axis of the complex). In such a system, the g, HF and quadrupole tensors are diagonal: $g_X = g_Y = g_\perp$, $g_Z = g_\parallel$,

Table 1. Parameters of the spin-Hamiltonian (2) measured at $T = 85$ K and two pressures, $P_0 = 0.1$ MPa and $P_1 = 550$ MPa (SHF tensor A is represented in the coordinate system whose axes, x'', y'' and z'', are coincident with eigenvectors of A; β_{exp} is the experimental value of the angle between the C_4 symmetry axis of the complex and the x'' axis).

	$P_0 = 0.1$ MPa	$P_1 = 550$ MPa
$g_\parallel$	2.4910 ± 0.0005	2.489 ± 0.001
$g_\perp$	2.083 ± 0.001	2.083 ± 0.001
$a_\parallel$ (MHz)	360 ± 3	348 ± 6
$a_\perp$ (MHz)	26 ± 1.5	27 ± 3
Q (MHz)	9 ± 1.5	6 ± 3
$A_{x''}$ (MHz)	96 ± 13	99 ± 6
$A_{y''}$ (MHz)	99 ± 6	102 ± 9
$A_{z''}$ (MHz)	403 ± 6	406 ± 9
β_{exp} (deg)	17 ± 0.5	20 ± 1

$a_X = a_Y = a_\perp$, $a_Z = a_\parallel$ and $Q_Z = -(Q_X + Q_Y)$. The values of these tensor components at $T = 85$ K are listed in table 1 for two pressures, $P_0 = 0.1$ MPa and $P_1 = 550$ MPa. Regarding the SHF tensors A_i, they are equivalent each to other and can be described by five independent constants. For instance, in the coordinate system represented in figure 1 the tensor A_1 has the form

$$\begin{pmatrix} A_{XX} & 0 & A_{XZ} \\ 0 & A_{YY} & 0 \\ A_{ZX} & 0 & A_{ZZ} \end{pmatrix}. \tag{3}$$

Other A_i tensors ($i = 2, 3, 4$) can be built by transforming the tensor A_1 by rotations belonging to the C_{4v} symmetry group. It will be noted in section 4 that antisymmetric parts of these tensors (determined by a single parameter $A^a = (A_{xz} - A_{zx})/2$) arise in the second order of the perturbation procedure. Neglecting A^a we can find a coordinate system, $x''y''z''$, where the tensor A_1 has a diagonal form. In the case under consideration, $z''(A_1)$ and $x''(A_1)$ lie in the XOZ plane while $y''(A_1)$ is perpendicular to this plane (see figure 1). Experimental tensor components of the tensor A_1, which is diagonalized by a rotation of the coordinate axes, are represented in table 1 (β_{exp} is the angle between Z and x''). Other spin-Hamiltonian parameters represented in table 1 correspond to the XYZ coordinate system. All these experimental parameters were determined at $T = 85$ K and hydrostatic pressures $P_0 = 0.1$ MPa and $P_1 = 550$ MPa.

When hydrostatic pressure is applied to the SrF_2:Cu^{2+} sample some changes in the structure of its EPR spectra are observed. Up to $T \approx 100$ K these changes correspond mainly to the pressure-induced alterations of the static spin-Hamiltonian parameters, which are associated with additional deformations of the equilibrium nuclear configuration of the $[CuF_4F_4]^{6-}$ complex. But we have found that hydrostatic pressure leads to an increase in the EPR linewidths as well.

Pressure-induced deformations of the complex are explicitly detected in variations of the SHF tensor components and, consequently, in variations of angular dependences of SHF splitting in the EPR spectra of the complex. Figure 2 shows the angular dependences of SHF splitting in the EPR spectra of $[CuF_4F_4]^{6-}$ complex due to SHF interactions with some fluorine ions. Curves, symmetric relative to the vertical line for $\theta = 90°$, correspond to $F^-(2)$ (or $F^-(4)$) while non-symmetric curves correspond to $F^-(1)$ (enumeration of the fluorine ions is in accordance with figure 1, rotation in the ZOX plane is considered). Full curves correspond to $P_0 = 0.1$ MPa and dashed curves to $P_1 = 550$ MPa. θ is the angle between magnetic field vector B_0 and the Z-axis. The curves are the results of a theoretical calculation with

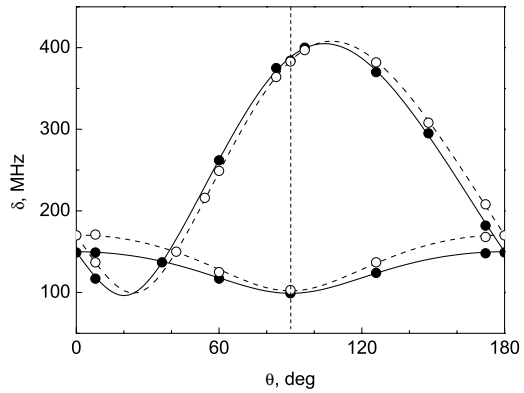

Figure 2. Angular dependences of the SHF splitting in EPR spectra of the $[CuF_4F_4]^{6-}$ complex at two pressures, $P_0 = 0.1$ MPa (full circles and full curves) and $P_1 = 550$ MPa (open circles and dashed curves); rotation in the ZOX plane (figure 1) is represented, curves which are symmetric relative to the vertical dashed line correspond to the ligands $F^-(2)$ and $F^-(4)$ while non-symmetric lines correspond to $F^-(1)$.

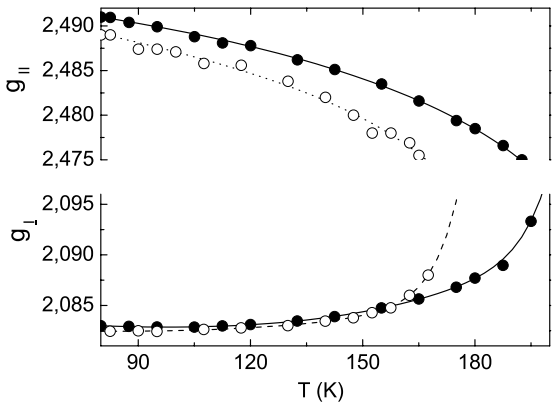

Figure 3. Temperature dependences of the $[CuF_4F_4]^{6-}$ complex's g-tensor components, $g_\parallel$ and $g_\perp$, for two pressures, $P_0 = 0.1$ MPa (full circles and full curves) and $P_1 = 550$ MPa (open circles and dotted curves).

the SHF tensor components from table 1 and the circles are experimental points (full circles correspond to P_0 and open ones to P_1). Analysing these angular dependences one can find that hydrostatic pressure induces variations of the SHF tensor components A_{ij} (see table 1). It is clear that the experimental values of these variations can give us rather detailed information about the equilibrium positions of nuclei of the $[CuF_4F_4]^{6-}$ complex. To get such information, a theoretical treatment based on the AOM LCAO MO approach was made and a short account of the results of this treatment will be described in section 4.1.

Besides the SHF tensor components, A_{ij}, the hydrostatic pressure induces some changes in g-tensor components ($g_\parallel$ and $g_\perp$). The character of these changes can be seen in figure 3 where the temperature dependences of $g_\parallel$ and $g_\perp$ are shown for $P_0 = 0.1$ MPa (full curves and full circles) and for $P_1 = 550$ MPa (dotted curves and open circles). One can see that each pair of curves represented in figure 3 tends towards merging into a single line. As was

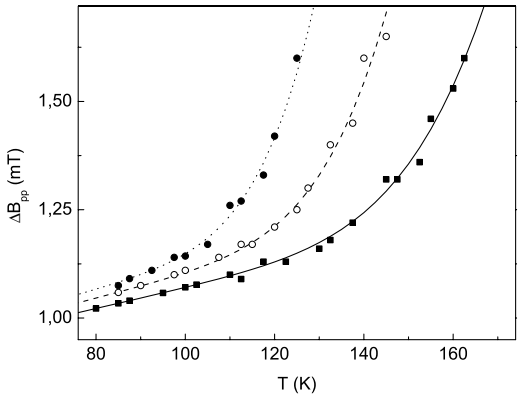

Figure 4. Temperature and pressure dependences of the cw EPR linewidth of the $[CuF_4F_4]^{6-}$ complex in SrF_2 crystal (full curve and squares correspond to pressure $P_0 = 0.1$ MPa, dashed curve and open circles to $P_1 = 300$ MPa, and dotted curve and full circles to $P_2 = 550$ MPa).

found for $P_0 = 0.1$ MPa in our previous work [2], this coalescence point corresponds to $g = (2g_\perp + g_\parallel)/3$. We assume here that this is also true for $P_1 = 550$ MPa (unfortunately we could not observe this merging process in our hydrostatic pressure experiments). It can be found from figure 3 that the coalescence point is shifted by a hydrostatic pressure of 550 MPa in the opposite direction along the temperature axis ($\Delta T \approx 20$–25 K).

Figure 2 (and figure 3, partly) shows experimental results associated mainly with static properties of the complex under consideration. Dynamic properties of this complex are represented more explicitly in the pressure and temperature variations of the EPR linewidth displayed in figure 4 and in the pressure shift of the coalescence point (figure 3). Temperature dependences of a peak-to-peak distance, $\Delta B_{pp}(T)$, of the low-field EPR line of EPR spectra recorded in parallel orientation of the $[CuF_4F_4]^{6-}$ complex at hydrostatic pressures $P_0 = 0.1$ MPa (full squares), $P_1 = 300$ MPa (open circles) and $P_2 = 550$ MPa (full circles) are represented in figure 4. One can see that the three curves represented in this figure have nearly identical shapes; they are shifted relative each to other and the maximal shift (for $\Delta P = P_2 - P_0$) is equal to $\Delta T \approx 25$ K.

4. Theoretical treatment of experimental results and discussion

4.1. Influence of hydrostatic pressure on the static spin-Hamiltonian tensor components

Due to the well-resolved SHF structure of EPR spectra of the $[CuF_4F_4]^{6-}$ complex there is the possibility of obtaining rather detailed information on the locations of the complex ions and their shifts under hydrostatic pressure. Symmetry of the SHF interaction with any of the four nearest ions is C_S and we have to analyse the quantities of the five SHF parameters A_{ij} included in the SHF tensor A_1 as the tensor components. It can be shown that, to first order of the perturbation theory, $A_{ij} \approx A_{ji}$ (see the text below). Starting this analysis we must note that the main features of the pressure dependences of the four independent tensor components are that the eigenvectors of a tensor A_i ($i = 1$–4) are rotated under pressure around the axis which is perpendicular to the symmetry plane (this is axis Y for the ligand $F^-(1)$ in figure 1). When the hydrostatic pressure reaches 550 MPa the rotation angle becomes nearly equal to 3°. It is surprising that the eigenvalues of the SHF tensor A_i are changed a little with pressure. As a consequence, the pressure dependence of isotropic part of the SHF tensor A_1 ($A_S = (A_{x'} + A_{y'} + A_{z'})/3$) is weak too ($\Delta A_S \approx 4$ MHz for $\Delta P = 550$ MPa, see table 1).

This means that the spin density of the unpaired electron localized on a ligand part of the complex ground antibonding molecular orbital (MO) is practically unaltered with a pressure. Thus, a rotation of the SHF tensor eigenvectors can be understood as a variation of the direction of the Cu^{2+}–$F^{-}(i)$-vector without significant change in the 'Cu^{2+}–$F^{-}(i)$' distances ($i = 1$–4). Taking into account the sign of this variation we can conclude that under pressure the Cu^{2+} ion moves toward the centre of its coordination cube.

For further backing for these qualitative conclusions we shall perform a semi-empirical treatment, which can provide us with more quantitative information on the pressure variation in the molecular structure of $[CuF_4F_4]^{6-}$. It must be noted that there is a large body of work concerned with theoretical treatment of covalent effects in ionic compounds (see, for example, [13–18] and references therein). Most of these works consider paramagnetic complexes belonging to the O_h, D_{4h} and D_{2h} symmetry groups. Symmetry of the SHF interactions in such a complex is D_{2h} or higher, and this is a reason why the results of these treatments cannot be directly applied to our case where the symmetry of the SHF interactions with the nearest ligands is C_S. The approach represented in [18] and [19] is more applicable. We shall use the results of this approach, translating them to LCAO MO terminology. Such a translation will simplify an understanding of the results of the theoretical treatment. In the following a short account of the treatment is presented.

Crystal field splitting of the orbital levels is determined with an effective Hamiltonian

$$H_{cf} = B_2^0 O_2^0 + B_4^0 O_4^0 + B_4^4 O_4^4. \tag{4}$$

The spin–orbit interaction determined by the operator

$$H_{SO} = L\lambda S \tag{5}$$

must be taken into account to estimate the coefficients in the ground Kramers doublet wavefunctions of the $[CuF_4F_4]^{6-}$ complex,

$$|\pm\rangle = \alpha_1|2, 2^S\rangle^{\pm} \mp \alpha_2|2, 2^A\rangle^{\pm} + \alpha_3|2, \mp 1\rangle^{\mp}, \tag{6}$$

where the basis MOs are the following:

$$|2, 2^S\rangle = |X^2 - Y^2\rangle = \frac{\sqrt{2}}{2}(|2, +2\rangle + |2, -2\rangle),$$
$$|2, 2^A\rangle = \mathrm{i}|XY\rangle = \frac{\sqrt{2}}{2}(|2, +2\rangle - |2, -2\rangle).$$

Coefficients of the linear combination (6) can be determined using second-order perturbation theory. In the case of the ground $|2, 2^S\rangle$ MO they satisfy the following equations:

$$\begin{aligned}
\alpha_1 &= 1 - \frac{\lambda_{1\perp}^2}{4\Delta E_2^2} - \frac{\lambda_{1\parallel}^2}{2\Delta E_1^2},\\
\alpha_2 &= \frac{\lambda_{1\parallel}}{\Delta E_1} + \frac{\lambda_{1\perp}^2}{2\Delta E_1 \Delta E_2},\\
\alpha_3 &= -\frac{\sqrt{2}\lambda_{1\perp}}{2\Delta E_2} - \frac{\sqrt{2}\lambda_{1\perp}\lambda_{1\parallel}}{2\Delta E_1 \Delta E_2} + \frac{\sqrt{2}\lambda_{1\perp}\lambda_{2\parallel}}{4\Delta E_2^2},
\end{aligned} \tag{7}$$

where the reduced spin–orbit interaction constants, $\lambda_{1\parallel}$, $\lambda_{2\parallel}$, $\lambda_{1\perp}$ and $\lambda_{2\perp}$, can be estimated neglecting spin–orbit interaction on the ligand orbitals (approximate relations see below).

Representing the electronic Zeeman interaction operator

$$H_Z = \beta_e B(L + g_s S) \tag{8}$$

on the wavefunctions (6) one can obtain the g-tensor components:

$$\begin{aligned} g_\parallel &= g_S(c_1^2 + c_2^2 - c_3^2) + 4k_{22}(c_1^2 - c_2^2) - 2k_{11}c_3^2, \\ g_\perp &= 2g_S c_1 c_2 + 4k_{21}c_1 c_3, \end{aligned} \tag{9a}$$

where

$$c_1 = \frac{\sqrt{2}}{2}(\alpha_1 - \alpha_2),\ c_2 = \frac{\sqrt{2}}{2}(\alpha_1 + \alpha_2) \text{ and } c_3 = \alpha_3.$$

In equations (9a), g_S is the g-factor of a free electron ($g_S = 2.0023$) and k_{ij} are the orbital reduction factors. Using equations (9a) and putting k_{22}, k_{11} and k_{21} equal to 1, approximate values of the coefficients α_1, α_2 and α_3, can be estimated from the experimental values of $g_\parallel$ and $g_\perp$. These values ($\alpha_1 = 0.9817$, $\alpha_2 = 0.0745$ and $\alpha_3 = 0.0331$) show that the ground state of the complex under study is represented mainly by the $|X^2 - Y^2\rangle$ MO.

Taking into account equations (7) one can transform equations (9a) to the following form:

$$\begin{aligned} g_\parallel &= g_S\left(1 - \frac{\lambda_{1\perp}^2}{\Delta E_2^2}\right) - 4k_{22}\left(\frac{2\lambda_{1\parallel}}{\Delta E_1} + \frac{\lambda_{1\perp}^2}{\Delta E_1 \Delta E_2}\right) - k_{11}\frac{\lambda_{1\perp}^2}{\Delta E_2^2}, \\ g_\perp &= 2g_S\left(\frac{1}{2} - \frac{\lambda_{1\parallel}^2}{\Delta E_1^2} - \frac{\lambda_{1\perp}^2}{4\Delta E_2^2}\right) - 4k_{21}\left(\frac{\lambda_{1\perp}}{2\Delta E_2} - \frac{\lambda_{1\perp}2_{2\parallel}}{4\Delta E_2^2}\right), \end{aligned} \tag{9b}$$

where the energy intervals ΔE_1 and ΔE_2 are determined by equations $\Delta E_1 = (E_{(XY)} - E_{(X^2-Y^2)})$ and $\Delta E_2 = (E_{(XZ,YZ)} - E_{(X^2-Y^2)})$. It must be noted here that, taking $k_{22} = k_{11} = k_{21} = 1$ and $\lambda_{1\parallel} = \lambda_{2\parallel} = \lambda_{1\perp} = \lambda$, one can transform equations (9b) to the form given by Bleaney *et al* [20].

The orbital reduction factors, k_{22}, k_{11} and k_{21}, are determined by the expression

$$k_{MM'} = \frac{\langle 2, M|L_j|2, M'\rangle}{\langle d_M|L_j|d_{M'}\rangle}. \tag{10}$$

In this expression, j corresponds to Z when $M = M'$ and to X when $M \neq M'$.

These orbital reduction factors will be estimated simultaneously with a treatment of experimental data for the SHF interactions.

In our case, the normalized basis molecular orbitals are

$$|L = 2, M\rangle = (N_{|M|})^{-1/2}(d_M - \chi_\sigma(M) - \chi_\pi(M)), \tag{11}$$

where the symmetry adapted linear combinations of p and s valence orbitals of the involved ligands ($\chi_\sigma(M)$ and $\chi_\pi(M)$) were obtained in the frame of the AOM [21, 22]. These combinations are as follows:

$$\begin{aligned} \chi_\sigma(M) &= \sum_{i=1}^{4} \mathrm{e}^{-\mathrm{i}M\varphi_i}\{F_M(\vartheta)[\lambda_s^D|0, 0\rangle_i - \lambda_\sigma^D|1, 0\rangle_i]\}, \\ \chi_\pi(M) &= \sum_{i=1}^{4} \mathrm{e}^{-\mathrm{i}M\varphi_i}\lambda_\pi^D\{\Phi_M(M)|1, +1\rangle_i + \Psi_M(\vartheta)|1, -1\rangle_i\}, \end{aligned} \tag{12}$$

where the angular functions $F_M(\vartheta)$, $\Phi_M(\vartheta)$ and $\Psi_M(\vartheta)$ are represented in table 2, φ_i and $\vartheta = \vartheta_i$ (i = 1–4) are the Euler angles of four equivalent fluorines (Cartesian coordinates as in figure 1), and λ_s^D, λ_σ^D and λ_π^D are the electron transfer parameters which can be determined by an analysis of the radial parts of the diatomic overlap integrals (S_s^D, S_σ^D and S_π^D).

Table 2. Angular functions included in equation (12).

M	$F_M(\vartheta)$	$\Phi_M(\vartheta)$	$\Psi_M(\vartheta)$
+2	$\sqrt{\frac{3}{8}}\sin^2\vartheta$	$-\frac{1}{2}\sin\vartheta(\cos\vartheta+1)$	$-\frac{1}{2}\sin\vartheta(\cos\vartheta-1)$
+1	$-\sqrt{\frac{3}{2}}\sin\vartheta\cos\vartheta$	$\frac{1}{2}(2\cos^2\vartheta+\cos\vartheta-1)$	$-\frac{1}{2}(2\cos^2\vartheta-\cos\vartheta-1)$
0	$\frac{1}{2}(3\cos^2\vartheta-1)$	$\sqrt{\frac{3}{2}}\sin\vartheta\cos\vartheta$	$-\sqrt{\frac{3}{2}}\sin\vartheta\cos\vartheta$
−1	$\sqrt{\frac{3}{2}}\sin\vartheta\cos\vartheta$	$-\frac{1}{2}(2\cos^2\vartheta-\cos\vartheta-1)$	$\frac{1}{2}(2\cos^2\vartheta+\cos\vartheta-1)$
−2	$\sqrt{\frac{3}{8}}\sin^2\vartheta$	$\frac{1}{2}\sin\vartheta(\cos\vartheta-1)$	$\frac{1}{2}\sin\vartheta(\cos\vartheta+1)$

The normalization coefficients $N_{|M_L|}$ of these MO are

$$\begin{aligned}
N_2 &= 1-\{\tfrac{3}{2}\sin^4\vartheta(\lambda_s^D S_s^D+\lambda_\sigma^D S_\sigma^D)+2\sin^2\vartheta(\cos^2\vartheta+1)\lambda_\pi^D S_\pi^D\}\\
&\quad+\{\tfrac{3}{2}\sin^4\vartheta[(\lambda_s^D)^2+(\lambda_\sigma^D)^2]+2\sin^2\vartheta(\cos^2\vartheta+1)(\lambda_\pi^D)^2\},\\
N_1 &= 1-12\sin^2\vartheta\cos^2\vartheta(\lambda_s^D S_s^D+\lambda_\sigma^D S_\sigma^D)\\
&\quad-(16\cos^4\vartheta-12\cos^2\vartheta+4)\lambda_\pi^D S_\pi^D\\
&\quad+\{6\sin^2\vartheta\cos^2\vartheta[(\lambda_s^D)^2+(\lambda_\sigma^D)^2]\\
&\quad+(8\cos^4\vartheta-6\cos^2\vartheta+2)(\lambda_\pi^D)^2\},\\
N_0 &= 1-(18\cos^4\vartheta-12\cos^2\vartheta+2)(\lambda_s^D S_s^D+\lambda_\sigma^D S_\sigma^D)\\
&\quad-24\sin^2\vartheta\cos^2\vartheta\lambda_\pi^D S_\pi^D\\
&\quad+\{(9\cos^4\vartheta-6\cos^2\vartheta+1)[(\lambda_s^D)^2+(\lambda_\sigma^D)^2]\\
&\quad+12\sin^2\vartheta\cos^2\vartheta(\lambda_\pi^D)^2\}.
\end{aligned}\tag{13}$$

When using these coefficients the approximate quantities of the effective parameters of spin–orbit interaction can be found as follows (in accordance with [23])

$$\begin{aligned}
\lambda_{1\|} &\approx N_2^{-1}\lambda,\\
\lambda_{2\|} &\approx N_1^{-1}\lambda,\\
\lambda_{1\perp} &\approx (N_2N_1)^{-1/2}\lambda,\\
\lambda_{2\perp} &\approx (N_1N_0)^{-1/2}\lambda,
\end{aligned}\tag{14}$$

where λ is the free Cu^{2+} ion spin–orbit interaction constant ($\lambda=-830\ \mathrm{cm}^{-1}$ [24]).

The Hamiltonian of the SHF interaction of an nl-electron with its nucleus may be written in the form [24, equation (17.30)]:

$$\boldsymbol{H}_{hfi}=g_s\beta_e\gamma_n\hbar\boldsymbol{I}\cdot\left\{\frac{\boldsymbol{l}}{r^3}-\frac{\boldsymbol{s}}{r^3}+3\frac{\boldsymbol{r}\cdot(\boldsymbol{s}\cdot\boldsymbol{r})}{r^5}+\frac{8}{3}\pi\boldsymbol{s}\delta(\boldsymbol{r})\right\}.\tag{15}$$

Representing this operator in the space of the ground Kramers wavefunctions (6) and using the relations (13) and (14) of [19] the SHF tensor components can be found.

Further we shall neglect the high-order terms in the expressions found for the SHF tensor components because our treatment is very approximate. For the sake of convenience we shall represent the SHF tensor in the space of the real ligand functions ($\boldsymbol{s}(i)$, $\boldsymbol{p}_x(i)$, $\boldsymbol{p}_y(i)$ and $\boldsymbol{p}_z(i)$) considering the ligand parts of the ground Kramers wavefunctions in the following form

$$|X^2-Y^2\rangle_L^{\pm}=\sum_{i=1}^{4}\{a_s(i)\boldsymbol{s}^{\pm}(i)+x(i)\boldsymbol{p}_x^{\pm}(i)+y(i)\boldsymbol{p}_y^{\pm}(i)-z(i)\boldsymbol{p}_z^{\pm}(i)\},\tag{16}$$

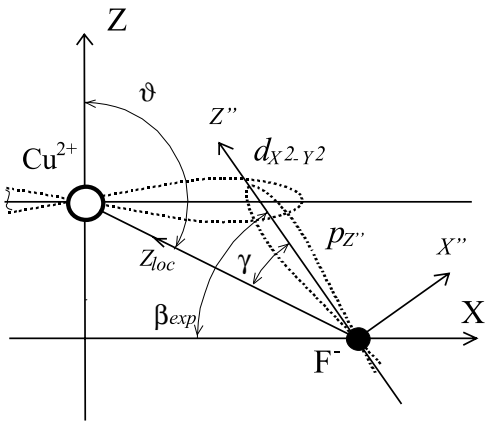

Figure 5. Reciprocal situation of the Cu^{2+} and $F^-(1)$ ions in the $[CuF_4F_4]^{6-}$ complex (the metal and ligand orbitals taking part in the ground $|X^2 - Y^2\rangle$ MO of the complex are presented).

where

$$\begin{aligned} a_s(i) &= (N_2)^{-1/2}\lambda_s^D \frac{\sqrt{3}}{2}\sin^2\vartheta\cos 2\varphi_i, \\ x(i) &= (N_2)^{-1/2}\lambda_\pi^D \sin\vartheta\cos\vartheta\cos 2\varphi_i, \\ y(i) &= (N_2)^{-1/2}(-\lambda_\pi^D \sin\vartheta\sin 2\varphi_i), \\ z(i) &= (N_2)^{-1/2}\lambda_\sigma^D \frac{\sqrt{3}}{2}\sin^2\vartheta\cos 2\varphi. \end{aligned} \tag{16a}$$

In this notation components of the SHF tensor A_1 ($\varphi_1 = 0°$) are the following (as the ligands F(1)–F(4) are equivalent, the index i will be omitted):

$$\begin{aligned} A_{XX} &\approx (a_s)^2 A_S^0 + (2x^2 - z^2)A_P^0, \\ A_{YY} &\approx (a_s)^2 A_S^0 - (x^2 + z^2)A_P^0, \\ A_{ZZ} &\approx (a_s)^2 A_S^0 + (2z^2 - x^2)A_P^0, \\ A_{XZ} &\approx A_{ZX} \approx 3xzA_P^0, \end{aligned} \tag{17}$$

where, for fluorine ions [13], $A_S^0 = 45.6$ GHz, $A_P^0 = 1.38$ GHz.

It must be pointed out here that the ligand functions ($\boldsymbol{p}_x(i)$, $\boldsymbol{p}_y(i)$ and $\boldsymbol{p}_z(i)$) are represented in the 'local' coordinate system with z_{loc} directed as shown in figure 5 (we call it 'local' as per convention). Equations (17) clearly show that, generally speaking, the axis z_{loc} cannot be considered as an eigenvector of the SHF tensor. To determine the 'Cu^{2+}–F^-' vector direction one needs an additional theoretical analysis. In the following we shall use the basic assumptions and statements of the AOM approach.

Let us consider a fragment of the $[CuF_4F_4]^{6-}$ complex which will consist of the impurity ion and a single ligand (for instance, the fluorine ion $F^-(1)$). These two ions lie in the XOZ plane of the coordinate system represented in figure 1. This fragment and the contours of electron spin densities of the unpaired electron localized at the ground $|X^2 - Y^2\rangle$ MO of the complex are shown qualitatively in figure 5, where ϑ is the Euler coordinate of the ligand $F^-(1)$ and z'' and x'' are the eigenvectors of the tensor A_1. It is obvious that one determines the angle β_{exp} by an EPR experiment. To determine the direction of z_{loc} one must take into account that the formation of a covalent bond leads to a lowering of the total energy of the system.

Further, one must transform the $d_{X^2-Y^2}$ and $p_{z''}$ functions (represented in figure 5) to the local coordinate system with axes x_{loc}, y_{loc} and z_{loc}. This transformation gives two covalent bond components (the σ and the π components). Thus, one can write for the covalent energy

$$E_{cov} = E_\sigma + E_\pi. \tag{18}$$

There is an approximate relation [25]

$$\frac{E_\sigma}{E_\pi} \approx \left(\frac{S_\sigma}{S_\pi}\right)^2 \tag{19}$$

which is frequently used in the AOM approach. Taking into account this relation and the symmetry of the bond under consideration one can get

$$E_{cov} \propto (S_\sigma + S_\pi)^2 \tag{20}$$

where S_σ and S_π can be represented in our case as products

$$S_\sigma = C_\sigma(\gamma)S_\sigma^D \qquad \text{and} \qquad S_\pi = C_\pi(\gamma)S_\pi^D. \tag{21}$$

Thus, the problem comes to solution of the equation

$$\left(\frac{\partial(S_\sigma + S_\pi)^2}{\partial\gamma}\right)_{R_{M-L}=\text{constant}} = 0. \tag{22}$$

(We must note here that the last conclusion was made neglecting the influence of the filled copper and fluorine orbitals. In fact, the energy of the complex depends on a mutual orientation of these orbitals too, but this dependence is weaker than the covalent effect [10].) Equation (22) leads to the relation

$$\operatorname{tg}\gamma = -\frac{2\sqrt{3}}{3}\operatorname{ctg}\vartheta\,\frac{S_\pi^D}{S_\sigma^D}. \tag{23}$$

One can find that the ratio S_σ^D/S_π^D depends on R_{M-L} rather weakly so that $R_{M-L} \approx 0.195$ nm may be considered as a trial quantity (the reasonableness of this figure will be shown below). Using equation (23) and taking into account the relation $\vartheta = \beta_{exp} - \gamma + 90°$, one can get $\gamma \approx 6°$ and $\vartheta \approx 101°$ for $P = 0.1$ Mpa, and $\gamma \approx 7.7°$ and $\vartheta \approx 102.5°$ for $P = 550$ MPa. As well as these angles, the calculations performed above give the following quantities:

$S_s^D = 0.042\,96$, $S_\sigma^D = -0.055\,21$, $S_\pi^D = 0.032\,96$, $\lambda_s^D = 0.092$, $\lambda_\sigma^D = -0.380$, $\lambda_\pi^D = 0.227$, $N_2 = 1.208$, $N_1 = 1.097$, $N_0 = 1.093$, $k_{22} = 0.829$, $k_{11} = 0.912$, $k_{21} = 0.711$, $\lambda_{1\parallel} = -687$ cm^{-1}, $\lambda_{2\parallel} = -758$ cm^{-1}, and $\lambda_{1\perp} = -721$ cm^{-1}. Values of these parameters do not conflict with those of found in [26] and [13]. It was found that these parameters are practically unchanged with pressure. The orbital energy intervals were found to be sensitive to pressure:

ΔE_1 (0.1 MPa) $\approx$ 8600 cm^{-1}, ΔE_2 (0.1 MPa) $\approx$ 9500 cm^{-1}, ΔE_1 (550 MPa) $\approx$ 8700 cm^{-1}, and ΔE_2 (550 MPa) $\approx$ 9600 cm^{-1}. We should say here that the value $R_{M-L} = 0.195$ nm adopted above was taken directly from [26]. But it is obvious that it needs confirmation. The following serves to do this.

As the value of R_{M-L} depends on the coordinates of the impurity Cu^{2+} ion and its ligands we shall try to find these coordinates, at least approximately. To estimate the displacements of eight fluorine ions of the $[CuF_4F_4]^{6-}$ complex arising due to off-centre shift of the impurity Cu^{2+}, we shall use the simplest model of an ionic crystal, the rigid-ion model (see, for instance, [11]). This model, based on the Born–Mayer type two-body potential, is frequently used to describe interactions in a solid:

$$V_{ij} = \frac{Z_i Z_j e^2}{r} + B_{ij}\exp\left(-\frac{r}{\rho_{ij}}\right) - \frac{C_{ij}}{r^6} \tag{24}$$

Table 3. Rigid-ion potential parameters for CaF_2 and SrF_2 (results of Bingham *et al* [27]).

	B (eV)	ρ (Å)	C (eV Å^6)
Ca^{2+}–F^-	797.42	0.3179	0
Sr^{2+}–F^-	715.41	0.3422	0
F^-–F^-	1127.7	0.2753	15.83

where Z_i is the ionic charge, r the separation of ions i and j and B_{ij}, ρ_{ij} and C_{ij} are constants of the potential. The first term describes the long-range Coulomb interaction between ions in the solid. The second term determines repulsive-type interaction due to an overlap of the electronic shells of these ions and the third term represents van der Waals dipole–dipole interaction. It is well known that rigid-ion potentials are satisfactory in molecular dynamic simulations and in determination of the energy of formation of various defects in ionic crystals [27]. They allow us to describe properties of the crystals using only a few parameters and this is an advantage in the use of such a rigid-ion model. We shall use the rigid-ion potential parameters found for CaF_2 and SrF_2 crystals and reported in [27] (see table 3).

It can be seen in table 3 that the van der Waals cation–anion interactions and the repulsive cation–cation and van der Waals cation–cation interactions are neglected in this approach. As for Cu^{2+}–F^-, Cu^{2+}–Ca^{2+} and Cu^{2+}–Sr^{2+} interactions, we have no available parameters to describe these. But we have some experimental data that can give us the possibility of obtaining them. First, for $[CuF_4F_4]^{6-}$ in SrF_2 we have calculated values of the angle ϑ for $P = 0.1$ and 550 MPa. The second experimental fact is that Cu^{2+} occupies a central position in the CaF_2 crystal. As long as there are fewer experimental data than parameters to be fitted, we have to make additional assumptions. Going along the lines of Bingham, Cormack and Catlow [27], we shall neglect the short-range Cu^{2+}–Ca^{2+} and Cu^{2+}–Sr^{2+} interactions. Of course, Cu^{2+} is a Jahn–Teller type ion and this latest assumption seems to be rather crude. But we have to restrict ourselves to such a model because we do not know any reported parameters for Cu^{2+} in fluorites. Calculations taking account of 96 ions and potentials described above give us $B(Cu^{2+}$–$F^-) = 343.4$ eV and $\rho(Cu^{2+}$–$F^-) = 0.3334$ Å. The impurity Cu^{2+} ion was found to be shifted from the on-centre position by 0.93 Å at $P = 0.1$ MPa and by 0.89 Å at 550 MPa. At $P = 0.1$ MPa the fluorine ions F(1–4) were found to be shifted toward the Cu^{2+} ion by 0.11 Å and fluorine ions F(5–8) shifted upward of Cu^{2+} by 0.14 Å. At $P = 550$ MPa these two latest values become 0.12 and 0.14 Å respectively. Thus, the distance 'Cu^{2+}–F^-(1)' was estimated to be equal to 1.97 Å at both pressures $P = 0.1$ and 550 MPa (this value is very close to the value used above in our calculations of the overlap integrals). It was also found that the energy of the complex in cubic configuration with the Cu^{2+} ion in the central position is higher than that for the configuration with Cu^{2+} in the off-centre tetragonal position. The energy difference between these molecular configurations is approximately 9×10^{-20} J (4500 cm^{-1}). Heights of the lowest barriers between adiabatic wells correspond to an energy difference of 3.2×10^{-20} J (1600 cm^{-1}). This latest result is comparable with the activation energy for interwell transitions of the $[CuF_4F_4]^{6-}$ complex reported in [2]. It must be noted that these heights are decreased with pressure $P = 550$ MPa by a factor of approximately 1.1.

Let us consider now the possible pressure variations of the 'impurity–ligand' distance, ΔR_{M-L}. Such a problem was considered in detail in [13]. One of the results of this consideration is that the isotropic part of the SHF tensor must be very sensitive to a variation of the 'metal–ligand' distance. But our experimental results show a practical independence of the isotropic part of the SHF tensor on pressure. In fact, the maximal change in the SHF isotropic constant was found to be approximately equal to 4 MHz while A_S (0.1 MPa) = 199 MHz

and A_S (550 MPa) = 203 MHz. To evaluate ΔR_{M-L} one can use the following approximate relation

$$\Delta R_{M-L} = \frac{1}{\partial(f_S)/\partial R_{M-L}} \frac{\Delta A_S}{A_S^0}, \tag{25}$$

where f_S is unpaired density transfer onto ns-orbitals of a ligand (in the notation of the present article f_S corresponds to $a_s(i)$ (see equations (17)) and $A_S^0 = 45\,600$ MHz). An approximate value for $\partial(f_S)/\partial R_{M-L}$ near to $R_{M-L} = 1.95$ Å can be found in figure 3 of [13]; it is approximately equal to 0.027 Å^{-1} (average value). Finally, one can get $\Delta R_{M-L} \approx 0.003$ Å. Thus, we can conclude that the metal–ligand distance is slightly changed with hydrostatic pressure, at least up to 550 MPa.

We now mention the pressure variations of the g-tensor components, $g_\perp$ and $g_\parallel$. The calculations performed with expressions (9b) show that the energy intervals ΔE_1 and ΔE_2 increase with pressure. This is not surprising since an overall compression of the crystal lattice must lead to an increase in the crystal field parameters B_2^0, B_4^0 and B_4^4.

4.2. Pressure and temperature dependences of the EPR linewidth

It is well known (see, for example, [28]) that EPR lines can be broadened homogeneously and/or inhomogeneously. Inhomogeneous line broadening is associated mainly with inhomogeneous external magnetic fields, unresolved HF and SHF structures, random strains in a crystal (which contains paramagnetic centres with anisotropic magnetic properties) and so on. Linewidth temperature dependences of the inhomogeneously broadened EPR lines are rather weak in most cases. But in some cases the inhomogeneous broadening processes can be strongly dependent on temperature. For instance, such case is realized in the anisotropic Jahn–Teller centres which can perform tunnelling transitions between the wells of a multiwell adiabatic potential. Simultaneously, this tunnelling process strongly influences the lifetimes of electron spin states of a Jahn–Teller centre and disturbs the precessional motion of the electron spin. Consequently, it leads to homogeneous broadening of the EPR lines.

Relations between the EPR linewidth of the $[CuF_4F_4]^{6-}$ Jahn–Teller complexes in SrF_2 crystals, the electron spin–lattice relaxation time (T_1) and the phase memory time (T_M) at normal atmospheric pressure were considered in previous work [2]. In the present discussion we shall analyse (taking into account these relations) the temperature dependences of the EPR linewidth established at various external pressures (0.1 MPa $\leqslant P \leqslant$ 550 MPa) in the present study. Within the experimental errors these dependences (represented in figure 4 in the form of graphs $\Delta B_{pp}(T)_P$ built for three particular pressures, $P_0 = 0.1$ MPa, $P_1 = 300$ MPa and $P_2 = 550$ MPa) can be well described by the following expression:

$$\Delta B_{pp}(T, P) = a(P) + b(P)T + c(P)\exp\left(-\frac{T_a(P)}{T}\right) \tag{26}$$

where the experimental parameters $a(P)$, $b(P)$ and $T_a(P)$ can be written in a common form

$$\begin{aligned} &(d(P) \to a(P), b(P), T_a(P)) \\ &d(P) \approx d_0 + d_1 P. \end{aligned} \tag{27}$$

The parameters introduced in equation (26) have the following values:

$$\begin{aligned} &a_0 \approx 0.83 \text{ mT}, && a_1 \approx 0, \\ &b_0 \approx 0.0024 \text{ mT K}^{-1}, && b_1 \approx 10^{-6} \text{ mT K}^{-1} \text{ MPa}, \\ &T_a \approx 1600 \text{ K}, && T_{a1} \approx -0.4 \text{ K MPa}^{-1}. \end{aligned}$$

We found the coefficient $C(P)$ to be nonlinear,

$$c(P) \approx c_0 + c_1(P)^{1.6} \tag{28}$$

where $c_0 \approx 7.1 \times 10^3$ mT and $c_1 \approx 0.65$ mT $(\text{MPa})^{-1.6}$.

It can be seen in figure 4 that the shapes of all three graphs $\Delta B_{pp}(T)_P$ represented in this picture are nearly identical. This means, that the reasons for the temperature dependences of $\Delta B_{pp}(T)_P$ observed in our experiments are the same. Thus, in the pressure range 0.1 MPa $\leqslant P \leqslant$ 550 MPa we can refer (assuming a Lorentzian shape for the EPR lines) to the relation [2]

$$\Delta B_{pp}\ (\text{mT}) \approx \frac{13.1302}{g T_2^*\ (\text{s})} \times 10^9, \tag{29}$$

where (in non-saturating conditions and at temperatures far enough from the g-factor coalescence point) the effective relaxation time T_2^* can be associated with the dynamic constants T_1 and T_M by the relation

$$\frac{1}{T_2^*} \approx \frac{1}{T_M} + \frac{1}{2T_1}. \tag{30}$$

In the temperature range where ΔB_{pp} becomes very strongly temperature dependent, the approach $T_M \approx T_1$ can be used. In this range (as it was found in [2]) the relaxation times T_M and T_1 are governed by tunnelling processes via the excited vibronic states and by over-barrier jumps. At $P_0 = 0.1$ MPa the two lowest excited vibronic states are separated from the ground state by the energy intervals $\Delta E_1 \approx 83\ \text{cm}^{-1}$ and $\Delta E_2 \approx 174\ \text{cm}^{-1}$ [2]. These experimental facts prove the intervals between these three lowest levels to be equidistant and the vibrations of the $[CuF_4F_4]^{6-}$ complex to be harmonic. This means that the potential barriers between potential wells are rather high. The vibrational frequency ω_i corresponding to a vibrational state E_i in an adiabatic well depends on the shape of the potential surface determining the values of the vibronic constants [29] $F_\Gamma^{\Gamma\Gamma'}$ (the linear vibronic constants), $K_{\Gamma'}^{\Gamma}$ (the force constants) and so on. By the shell model calculations it was shown [30] that the shape of the adiabatic potential surfaces of non-central Li^+, Cu^+ and Ag^+ impurity ions in the alkaline halide crystals depends strongly on hydrostatic pressure. Our calculations performed using the shell model approach (a short description has been given above; a fuller account can be found in [31]) show that the bottom curvature of the ground adiabatic potential sheet of the $[CuF_4F_4]^{6-}$ complex and the heights of potential barriers are decreased under hydrostatic pressure. This leads to a decrease in the force constants $K_{\Gamma'}^{\Gamma}$ and, consequently, to a decrease in vibronic frequencies ω_i. Thus, when hydrostatic pressure acts on the crystal under study population of the excited vibronic states must start at lower temperatures. It was found [31] that the overlap integrals of the excited vibronic wavefunctions are practically independent of hydrostatic pressure (due to a decrease in the potential barriers with pressure). Thus, one can conclude that the tunnelling processes must be accelerated with increased pressure and such acceleration leads to an increase in the EPR linewidth.

Of course, there is another mechanism for pressure dependence of the EPR linewidth, associated with the compression of the crystal lattice. This compression leads to expansion of the lattice phonon spectrum and, consequently, can partly account for the temperature and pressure dependences of the EPR linewidth observed in the experiment. But there is an additional experimental fact suggesting pressure-induced shift of the impurity ion to the centre of its coordinational polyhedron. This shift changes the shape of the lowest adiabatic potential sheet and alters the conditions of the tunnelling process. Obviously, this latest mechanism becomes dominant in the high-temperature region at high pressures.

5. Conclusions

As has been shown in the preceding section, hydrostatic pressure significantly influences the properties of the non-central Jahn–Teller $[CuF_4F_4]^{6-}$ complex in an SrF_2 crystal. Both the static and dynamic parameters of the complex are altered with pressure. A change in static parameters is associated mainly with pressure deformations of the equilibrium molecular configuration of the complex. Under the action of hydrostatic pressure the four nearest ligands move toward the impurity ion. This results in motion of the copper ion to the centre of its coordination polyhedron and in an increase in the Euler coordinates, ϑ_i, of these four ligands. Such an effect of pressure on the molecular structure of the complex changes both the curvature of the adiabatic well surface and the heights of the potential barriers. As the result, the vibronic frequencies of the complex are decreased while the phonon spectrum of the crystal lattice (due to a compression of the lattice) is extended. These processes lead to acceleration of the tunnelling transitions of the complex with increasing pressure.

Acknowledgment

This work was supported partly (VAU) by the Russian Foundation of Basic Research (grant 01-02-17718).

References

[1] Zaripov M M and Ulanov V A 1989 *Fiz. Tverd. Tela* **31** 254
[2] Hoffmann S K and Ulanov V A 2000 *J. Phys.: Condens. Matter* **12** 1855
[3] Ulanov V A, Zaripov M M and Zheglov E P 2002 *Fiz. Tverd. Tela* **44** 1410
[4] Bill H 1973 *Phys. Lett.* A **44** 101
[5] Bill H, Millert C M and Lacroix R 1973 *Proc. 17th Congr. AMPERE* p 233
[6] Moreno M 1974 *Ann. Phys. Real. Soc. Esp.* **70** 261
[7] Studzinski P, Casas-Gonzales J and Spaeth J M 1984 *J. Phys. C: Solid State Phys.* **17** 5411
[8] Alonso P J, Casas-Gonzales J, den Hartog H W and Alcala R 1983 *Phys. Rev.* B **27** 2722
[9] Shannon R D and Previtt C T 1969 *Acta Crystallogr.* B **25** 925
[10] Gerloch M and Slade R C 1973 *Ligand Field Parameters* (Cambridge: Cambridge University Press) p 236
[11] Sangster M J L and Dixon M 1976 *Adv. Phys.* **25** 247
[12] Krupski M 1996 *Rev. Sci. Instrum.* **67** 2894
[13] Moreno M, Barriuso M T and Aramburu J A 1992 *Appl. Magn. Reson.* **3** 283
[14] Shulman R G and Sugano S 1963 *Phys. Rev.* **130** 517
[15] Hubbard J, Rimmer D E and Hopgood F R A 1966 *Proc. Phys. Soc.* **88** 13
[16] Owen J and Thornley J H M 1996 *Rep. Prog. Phys.* **29** 675
[17] Polak K and Malek J 1972 *Czech. J. Phys.* B **22** 1232
[18] Eremin M V 1990 *Opt. Spectrosc.* **68** 860
[19] Eremin M V, Ulanov V A and Zaripov M M 1998 *Appl. Magn. Reson.* **14** 435
[20] Bleaney B, Bowers K D and Price M H L 1955 *Proc. R. Soc.* A **228** 166
[21] Schaffer C E 1968 *Struct. Bond.* **5** 68
[22] Rakitin Yu V and Kasumov R D 1985 *Coord. Chem.* **11** 867 (in Russian)
[23] McGarvey B R 1976 *J. Chem. Phys.* **65** 955
[24] Abragam A and Bleaney B 1970 *Electron Paramagnetic Resonance of Transition Ions* (Oxford: Clarendon) p 911
[25] Smith D W 1977 *Inorg. Chim. Acta* **22** 107
[26] Kubo H, Kaneshima N and Hirakawa K 1976 *J. Phys. Soc. Japan* **41** 1165
[27] Bingham D, Cormack A N and Catlow C R A 1989 *J. Phys.: Condens. Matter* **1** 1205
[28] Weil J A, Bolton J R and Wertz J E 1994 *Electron Paramagnetic Resonance. Elementary Theory and Practical Applications* (New York: Wiley) p 1568
[29] Bersuker I B 1996 *Electronic Structure and Properties of Transition Metal Compounds. Introduction to the Theory* (New York: Wiley) p 668
[30] Holland U and Luty F 1979 *Phys. Rev.* B **19** 4298
[31] Ulanov V A, Nikiforov A E, Chernyshev V A and Zhiteitsev E R 2003 *Appl. Magn. Reson.* **22** at press